

Bayesian framework for non-destructive post-fire assessment of reinforced concrete beams using the incremental neutral axis position

Balša Jovanović, Jasper Godeau, Robby Caspeepe, Edwin Reynders, Geert Lombert, Ruben Van Coile

Abstract

Post-fire assessment in concrete structures is a complex challenge. This study addresses this challenge, by incorporating an innovative technique that employs Fiber Bragg Gratings (FBGs) to measure strains at the top and the bottom of a beam and analyse them into a Bayesian inference framework. The FBGs allow to determine the position of the incremental neutral axis under bending deformation. The change of position of the incremental neutral axis relates to the degradation of concrete stiffness induced by fire, providing a key indicator of the structural condition of the whole member. The Bayesian methodology allows for a systematic handling of uncertainties, integrating prior knowledge with new data to improve the assessment's accuracy. By combining FBG-based strain sensing and advanced concrete modelling within a Bayesian framework, a novel approach is proposed to tackle the high uncertainties of post-fire assessments and deliver more reliable predictions than existing techniques. This offers a structured framework for interpreting the measured data and predicting the structural health of fire-affected concrete structures. To enable Bayesian inference, a numerical model is developed to calculate the incremental neutral axis position during and after fire. The model evaluates all the strain components, both reversible and irreversible and aggregates them to calculate the neutral axis position. The model's capabilities are validated using experimental data. The application of this methodology to a demonstration case shows its potential. The results show that employing the assessment technique can provide information on both the fire exposure, material properties of the member and its residual capacity. It highlights the feasibility of using FBG-based measurements for the post-fire assessment of concrete structures and underscores the value of Bayesian methods in managing the uncertainties inherent in such evaluations.

1. Introduction

Fires within the built environment can severely affect structural integrity and occupant safety. While it is common for concrete structures to withstand fires without experiencing complete collapse, the aftermath often reveals notable damage that can impair performance and residual service life [1]. Therefore, a thorough post-fire assessment must be conducted in order to accurately assess the structure's residual capacity and safety level [2].

Fire exposure is a highly complex phenomenon, with multiple sources of uncertainty that influence post-fire evaluations. These uncertainties include various aspects relevant to fire dynamics, such as the combustible fuel load and the ventilation conditions. Furthermore, there are uncertainties in the material properties of the structure itself. The presence of these uncertainties necessitates a detailed probabilistic approach when conducting post-fire assessment. Common practices, such as visual inspections and a combination of concrete core sampling, rebar testing, and non-destructive tests like the rebound hammer, are affected by uncertainties originating from the complex nature of fire damage and the nature of the assessment techniques [3]. By recognising and addressing these uncertainties, engineers can enhance the reliability of post-fire assessment, ensuring that the safety level of the structure post-fire is sufficient for continued use [4].

Concrete members experience permanent damage during fire in the form of reduction of material properties, cracking and residual strains. A promising approach is to use damage identification techniques based on strain measurements, leveraging the principle that changes in a structure's behaviour when experiencing small deformations can reveal damage. This approach is promising considering its non-destructive application and ability to detect hidden damage without prior knowledge of damage locations. However, its successful application is contingent on the sensitivity of the measured characteristics to the sustained damage. Recent applications of multiplexed Fiber Bragg Grating (FBG) sensors for measuring dynamic macro-strains present a breakthrough for such strain-based damage identification. An approach for using FBG measurements for damage detection in concrete structures has recently been developed [5]. This method relies on an evaluation of the strain mode shapes and employing them in order to calculate the position of the neutral axis. Its application as a possible tool for the post-fire assessment of a fire-damaged structure has been recently explored in [6].

An open problem in this regard is that the post-fire assessment methodology should effectively consider the uncertainties related to material properties and fire conditions. Bayesian updating techniques thus emerge as a potential solution by updating these uncertainties based on observed data [7]. Coupled with this strain-based damage identification, this methodology can enhance the estimation of the remaining structural capacity post-fire.

In the present study, an assessment technique based on the incorporation of strain measurements into a Bayesian updating framework is developed and its effectiveness is examined. The FBGs allow determination of the incremental neutral axis under bending, which reflects fire-induced degradation of stiffness across the full cross-section—providing a global damage metric often missed by conventional surface or point-based tests. Firstly, the FBG sensors are introduced together with an explanation of how they are employed to detect damage in a concrete member. Next, the notion of the incremental neutral axis as an indicator of the beam's condition is introduced. To further explore this, a detailed analysis of how strains are affected by fire-induced damage is presented together with a modelling approach. After this, the methodology for employing strain measurements coupled with Bayesian inference is introduced. By combining FBG-based strain sensing and advanced concrete modelling within a Bayesian framework, a novel approach is proposed to tackle the high uncertainties of post-fire assessments and deliver more reliable predictions than existing techniques. Finally, the complete approach is demonstrated in an experimental case study.

2. Strain measurements using Fiber Bragg Grating sensors

Fiber Bragg Grating (FBG) sensors are a type of optical fibre sensor used for measuring strain, temperature, and other physical parameters. They are made from glass fiber optical wires consisting of a core and cladding. Within the core, a series of grating planes are created through exposure to an intense ultraviolet (UV) laser. This changes the refractive index of the core, forming the FBG. The fundamental principle of FBGs is based on Bragg diffraction, where most of the light propagating through the fibre is transmitted, but a narrow band of optical wavelengths is reflected on the grating planes. The central wavelength of this reflected band is known as the Bragg wavelength [5].

FBG sensors offer several advantages, including ease of installation, resistance to harsh environments, long-term stability, the ability to multiplex (i.e., many different sensors can be inscribed into the same glass fibre) and relatively low cost. Due to their high precision and fast response, they have been employed as the basis of a novel damage assessment approach developed at KU Leuven [5] which focuses on detecting the position of the neutral axis using two sets of FBGs.

2.1. Neutral axis position

The evaluation of the neutral axis position using FBGs can be explained using the following case. In the example in Figure 1, a concrete beam with a symmetrical cross-section is presented. In the situation at the top, the beam is undamaged. When exposed to a sufficiently small positive moment M which tensions the bottom side of the beam, the material behaves elastically and symmetrically both in compression and tension. This then causes a symmetrical and linear total strain diagram, with the position of the neutral axis in the centroid of the cross-section (here considered to be at mid-height).

If the beam is damaged, its behaviour changes. Consider a situation with bending cracks in the tensioned zone. The tensile stiffness of the zone decreases and the total strain diagram for the same applied moment differs. In this case,

due to the higher deformations in the bottom (tensile) zone, the position of the neutral axis is higher than the section's centroid. This demonstrates that the position of the neutral axis is influenced by the damage experienced by the member.

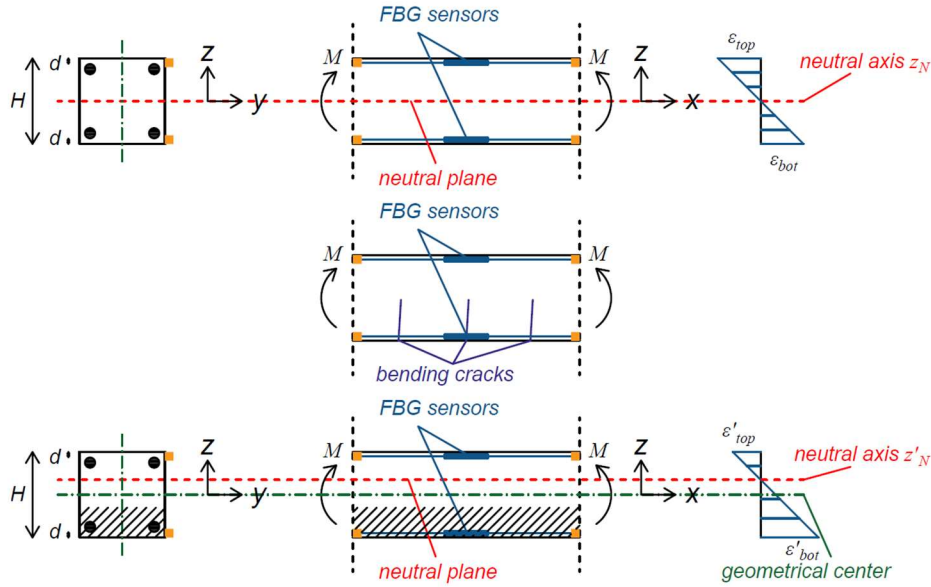


Figure 1. Illustration of the use of strain mode shapes to detect damage to the concrete beam.[5]

Using FBGs, the position of the neutral axis can be calculated. FBGs can be employed for measuring the average longitudinal strain (or macrostrain) at a specific location of the cross-section of a beam element, as the sensor measures the relative deformations between the two attachment points to the beam. This way, the focus is on the long-gauge strains as they relate to a smeared crack model. This model allows the use of the Euler-Bernoulli hypothesis in damaged condition, which states that plane cross-sections before deformation remain plane and normal to the beam's axis after deformation. If two sensors are attached, one in the compressed and one in the tensioned zone, the total linear strain diagram can be approximated. The position of the neutral axis can then be obtained using the following formula:

$$NA = \frac{\varepsilon_{bot} + \varepsilon_{top}}{\varepsilon_{bot} - \varepsilon_{top}} \cdot \frac{d}{2} + \frac{a_{bot} - a_{top}}{2} \quad (1)$$

where NA is the position of the neutral axis relative to the centre of the cross-section, ε_{top} and ε_{bot} are measured longitudinal strains at the top and bottom for the cross-section respectively, d is the distance between them and a_{bot} and a_{top} are distances of the measuring points from the closest edge.

This approach can also be applied in dynamic testing. In this case, the applied static moment is replaced by a dynamic excitation. This excitation causes bending and a change in the total strain diagram. Instead of the instantaneous values of the strain, strain mode shapes can be used. For each sensor (top and bottom) a strain mode shape can be determined. Unlike displacement mode shapes, which depict how parts of a structure move in space during a vibration cycle, strain mode shapes represent how parts of the structure deform or strain during a vibration cycle. Strain mode shapes have the advantage of allowing the decoupling of bending deformations from other types of deformations. Additionally, since they are derived from dynamic measurements, the FBGs do not require temperature compensation if adequately protected. They also require only very small loading amplitudes and natural frequencies are determined along with the strain mode shapes from the same FBG data. When these strain mode shapes are implemented in Eq. (1) the position of the neutral axis along the whole beam can be obtained.

The central hypothesis explored in the current paper is that this method can be used for post-fire assessment of concrete members. This is due to the fact that, similarly to bending damage indicated in Figure 1, fire damage is usually also not symmetrical and affects the beam area closer to the fire more severely. Thus, in the following, the possible application of this technique is going to be examined from a theoretical perspective.

2.2. Incremental neutral axis position

In order to properly use the neutral axis position as a technique for post-fire assessment, its behaviour has to be properly defined and modelled. The FBGs are measuring the macrostrain at the top and bottom of the beam due to the additional beam deformation. It must be stressed that the FBGs are not measuring the beam's total strains at those positions, but the difference between the unloaded and loaded state. Therefore, the neutral axis position that is obtained using Eq. (1) is not the actual neutral position, but an incremental neutral axis position associated with the additional deformation. When the beam is excited, it deforms and therefore, the total strain diagram at every cross-section changes. As the total strain diagram is linear across the height of the cross-section, considering the Euler-Bernoulli hypothesis, it can be defined in the following way:

$$\varepsilon_{tot} = -\chi \cdot y + \varepsilon_0 \quad (2)$$

where ε_{tot} represents the total strain at a position y , χ is the cross-sectional curvature, y is the vertical position in reference to the centre of the cross-section and ε_0 is the strain in the centre of the cross-section (where $y = 0$). In the case of a small deformation the total strain at the positions of the FBGs is equal to:

$$\begin{aligned} \varepsilon_{top} + d\varepsilon_{top} &= -(\chi + d\chi) \cdot y_{top} + (\varepsilon_0 + d\varepsilon_0) \\ \varepsilon_{bot} + d\varepsilon_{bot} &= -(\chi + d\chi) \cdot y_{bot} + (\varepsilon_0 + d\varepsilon_0) \end{aligned} \quad (3)$$

where the operator d represents a small differential change. The terms $d\varepsilon_{top}$ and $d\varepsilon_{bot}$ are the values that are obtained from the measurements. When substituting those two terms in Eq. (1), one finds that the incremental neutral axis position actually represents the first derivative of average strain by curvature:

$$dNA = \frac{d\varepsilon_0}{d\chi} \quad (4)$$

Although the incremental neutral axis position was originally obtained based on the strain mode shapes [5], it can also be derived from static strain measurements, considering the change in strains at the top and bottom of the beam under small bending deformation. Furthermore, other techniques that can capture long-gauge strains, such as Digital Image Correlation (DIC) can also be employed.

In order to properly understand the behaviour of this incremental neutral axis position, strain distributions inside the concrete member must be quantified.

When applied in situ, the FBGs would be attached (e.g. by glueing [23] or clamping [5,6]) to the top and the bottom edge of the fire-affected beam. A small amplitude bending load is imposed (e.g. via a calibrated hydraulic jack) to generate incremental strain responses while preserving the structure's post-fire condition. At two or three discrete load levels, longitudinal strains at the top and bottom faces are recorded, and their differences are substituted into Eq. (1) to determine the in situ position of the incremental neutral axis. This procedure, requiring only readily deployable instrumentation, can be completed within a few hours, thus enabling quick post-fire assessment.

3. Modelling of the post-fire position of the neutral axis

The measured position of the neutral axis does not provide direct information on the condition of the beam after the fire exposure. The neutral axis position is, however, influenced by the same parameters that govern the residual condition, such as the fire exposure and material properties of concrete and reinforcement. To infer information on these influencing parameters from a neutral axis position measurement, a Bayesian updating framework can be employed. Through the Bayesian updating framework, prior knowledge is updated considering new information. Here, the Bayesian approach enables a probabilistic assessment of the fire exposure and material properties, providing additional input for the post-fire evaluation and thus enhancing the accuracy of the structural evaluation post-fire.

The development and application of the conceptual Bayesian framework outlined above requires a model that establishes a quantitative relationship between the fire exposure and material properties on the one hand, and the neutral axis position on the other hand. Thus, a model connecting the fire exposure and material properties with the position of the neutral axis has been developed. The model encompasses a fire curve, heat transfer, strain calculation and neutral axis position evaluation. The connection between these parts is illustrated in Figure 2. First, the fire curve is evaluated starting from input values for the opening factor and the fuel load density. Then, a heat transfer analysis is performed to evaluate the temperatures within the concrete cross-section. For each time step, the strains in the cross-section are modelled taking into account the material properties as well as the load on the structure. Finally, when the full time-history of fire exposure has been considered, the residual strains and post-fire neutral axis position are determined and compared with the neutral axis position determined based on the FBGs. In the following, these components are introduced together with the results of the strain (deformation) model validation based on the experimental results.

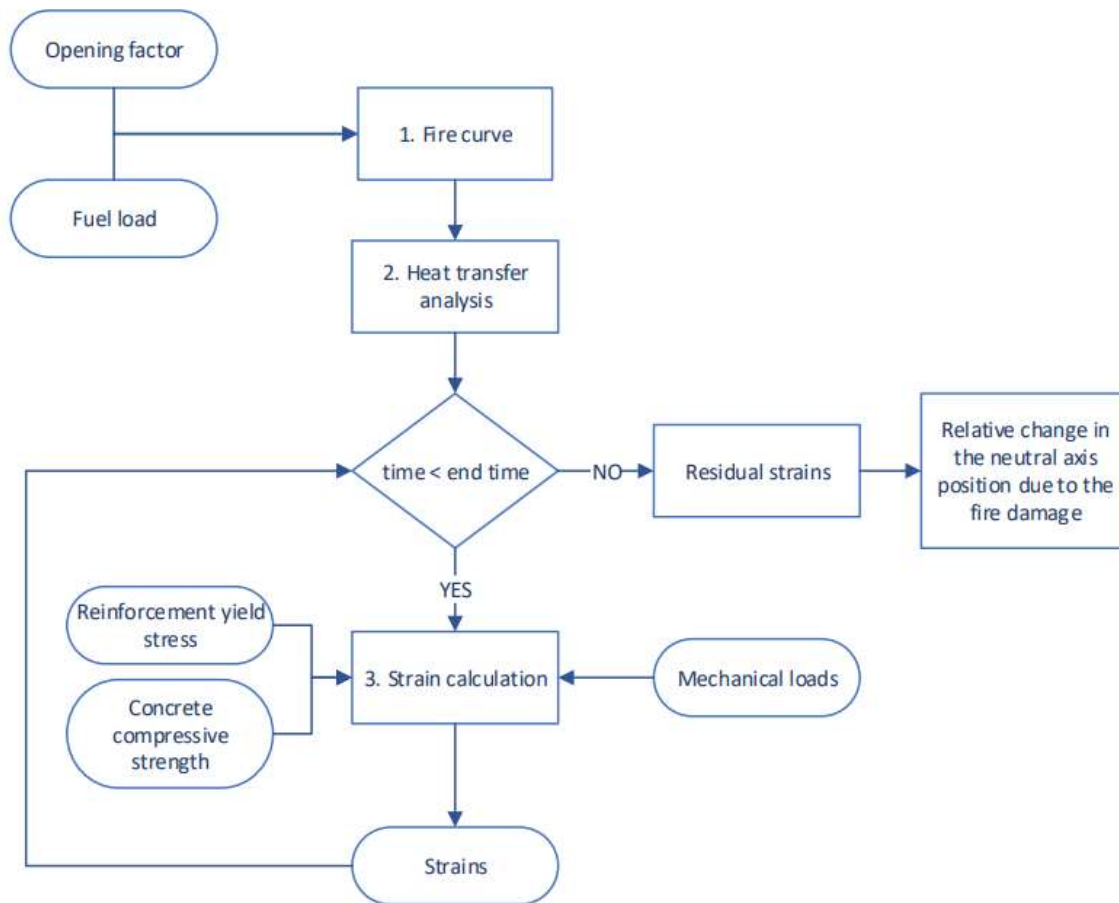


Figure 2. Flowchart of the neutral axis position calculation model

3.1. Fire curve

The fire curve can be understood as an engineering model for fire exposure. In this work, the Eurocode Parametric Fire Curve (EPFC) [8] is used. This representation of the fire exposure is commonly used in Structural Fire Engineering (SFE) and it defines the temperature-time curve of the hot gases in the compartment during a post-flashover fire. This curve is a function of the ventilation conditions through the opening factor O , available fuel during the fire through the fuel load density q_f , thermal properties of the compartment linings through the thermal effusivity

b and geometry of the compartment through its dimensions. The curve consists of two phases, heating and cooling, making it applicable for use in post-fire assessment.

3.2. Heat transfer

In order to model the heat transfer inside of the concrete member, a finite difference method is employed. This method consists of discretizing the cross-section into smaller elements and solving heat transfer equations in order to obtain a temperature field during the whole heating and cooling periods. The finite difference method allows for an easy and computationally efficient integration in the total workflow (Python coding). The results were validated against commercial finite element software. As available experimental data where FBG measurements have been used as part of a post-fire assessment [16] considers one-sided exposure, this exposure condition is considered in the remainder of this paper and a one-dimensional heat transfer model is adopted. The thermal properties of concrete described in EN 1992-1-2 [9] are used. The EPFC's effect is introduced as a combination of convective and radiative heat transfer with a convective heat coefficient of 35 kW/m² and emissivity of 0.7. The post-fire cooling considers irreversible thermal properties and the same boundary conditions

3.3. Strain component modelling

3.3.1. Concrete strain distribution

For concrete at ambient conditions, the total strains consist of the following components:

$$\varepsilon_{tot} = \varepsilon_{mech} = \varepsilon_{el} + \varepsilon_{pl} \quad (5)$$

where ε_{mec} represents mechanical strains which consist of an elastic ε_{el} and plastic part ε_{pl} . Plastic strain is irreversible and will not occur in case of small deformations. However, it will have to be taken into account when determining the elastic strains from the total strains.

If the concrete has been subjected to heating, the total strain has to take into account additional components:

$$\varepsilon_{tot} = \varepsilon_{el} + \varepsilon_{pl} + \varepsilon_{th} + \varepsilon_{tr} \quad (6)$$

where ε_{th} is the thermal strain and ε_{tr} is the transient creep strain. The thermal strain occurs as the concrete expands due to the increase in temperature. Transient creep strain is an additional irreversible strain that occurs in concrete when it is exposed to compression during heating [10]. Out of all these components, only the elastic strain and part of the thermal strain are reversible after the fire exposure and therefore, the total post-fire strain can be presented as a sum of residual and elastic strain:

$$\varepsilon_{tot} = \varepsilon_{el} + \varepsilon_{res} = \varepsilon_{el} + \varepsilon_{pl} + \varepsilon_{th,res} + \varepsilon_{tr} \quad (7)$$

where ε_{res} represents the sum of all residual (irreversible) strains and $\varepsilon_{th,res}$ represents the residual part of the thermal strains ε_{th} (one that remains after the material cools to ambient temperature). These strains play a crucial role in determining the position of the incremental neutral axis and are explained in detail in the following text.

The strain calculation is conducted using a cross-sectional analysis. The whole cross-section is divided into the same sections as in the heat transfer analysis. For every time step, the stress distribution is calculated as a function of the total strain distribution and temperature. By integrating the stresses, both the axial force and the bending moment are obtained. The cross-sectional analysis thus provides a relationship between the internal forces and the total strain diagram parameters, i.e., the curvature and strain at the centre. Therefore, if the internal forces are known, the total strain and subsequently all its component's distributions over the cross-section can be obtained. The process is illustrated in Figure 3.

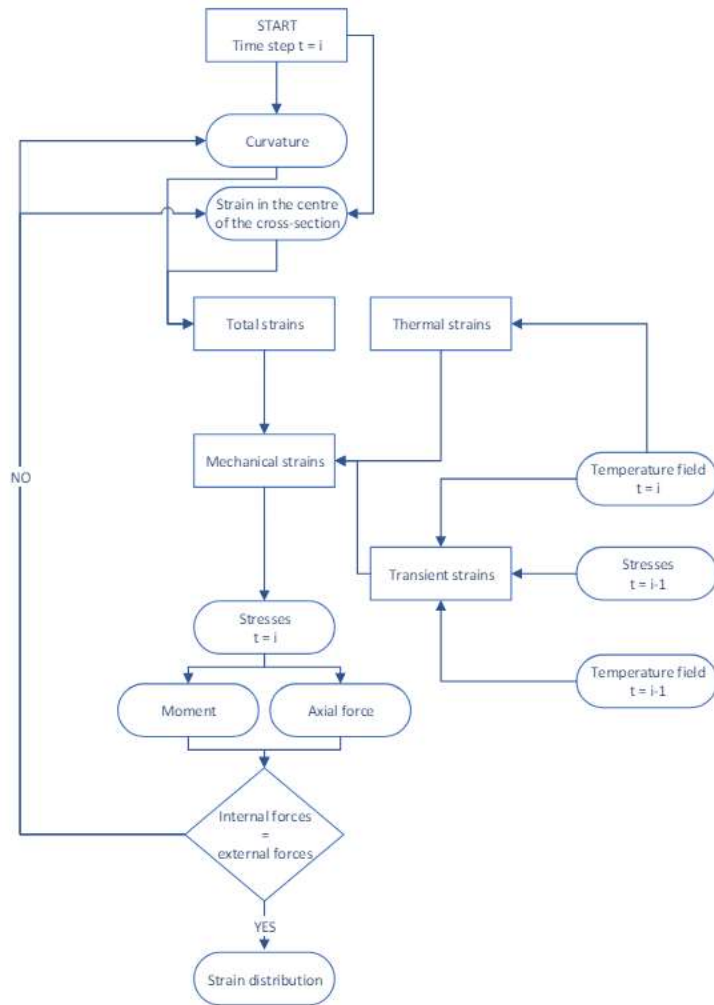


Figure 3. Flowchart representing the strain calculation model for a given time step i

All the components of the total strain are influenced by either or both the stress or temperature-time history. For this reason, the analysis has to be conducted for all points in time during the fire exposure. The progression of strain components is logged at every time step, as described in the following.

3.3.2. Thermal strain

The thermal strain during the heating phase (before the element has reached its maximum temperature) is modelled as a function of the current temperature of the element, adopting the model defined in [9]. During cooling, it is a function of both the current temperature and the maximum temperature the element experienced, according to the formulation in [11]. This is represented in Figure 4.

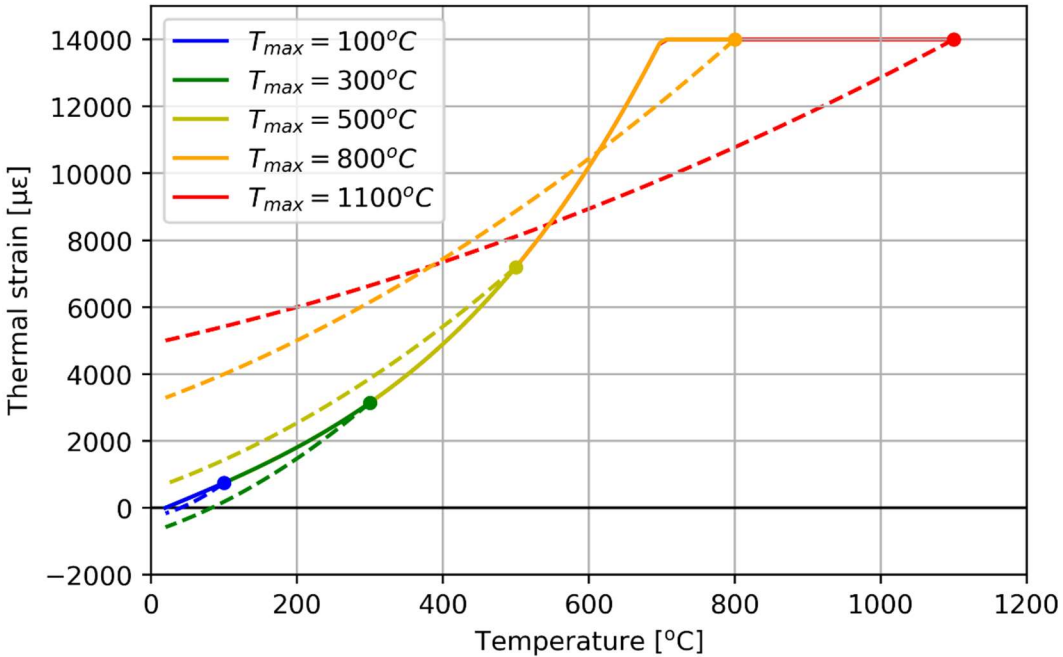


Figure 4. Thermal strain evolution during the heating up to temperature T_{max} , and subsequent cooling. The dashed line represents the cooling phase

3.3.3. Mechanical strains

Mechanical strains are modelled based on their relationship with stresses. Concrete stresses are modelled as defined in EN 1994-1-2 [12] (including additional strength reduction during cooling), as a function of mechanical strains and the temperature-time history of the element. In the case of unloading (decrease of the compressive mechanical strains), the slope of the descending branch is equal to the tangential modulus of elasticity at the origin based on the maximum experienced temperature [13]. This loading-unloading scenario is presented in Figure 5, where the stress-strain history for two elements is plotted, one which remained at ambient temperature and the other for an element that previously experienced temperatures up to 300 °C. Using this descending branch, the mechanical strain can be divided into its elastic and plastic components, where the plastic one is defined as irreversible. Furthermore, the ultimate tension strain is monitored throughout the whole simulation. If this value is exceeded, the element is considered cracked, meaning that if it is exposed to tensile strains, stresses are equal to zero.

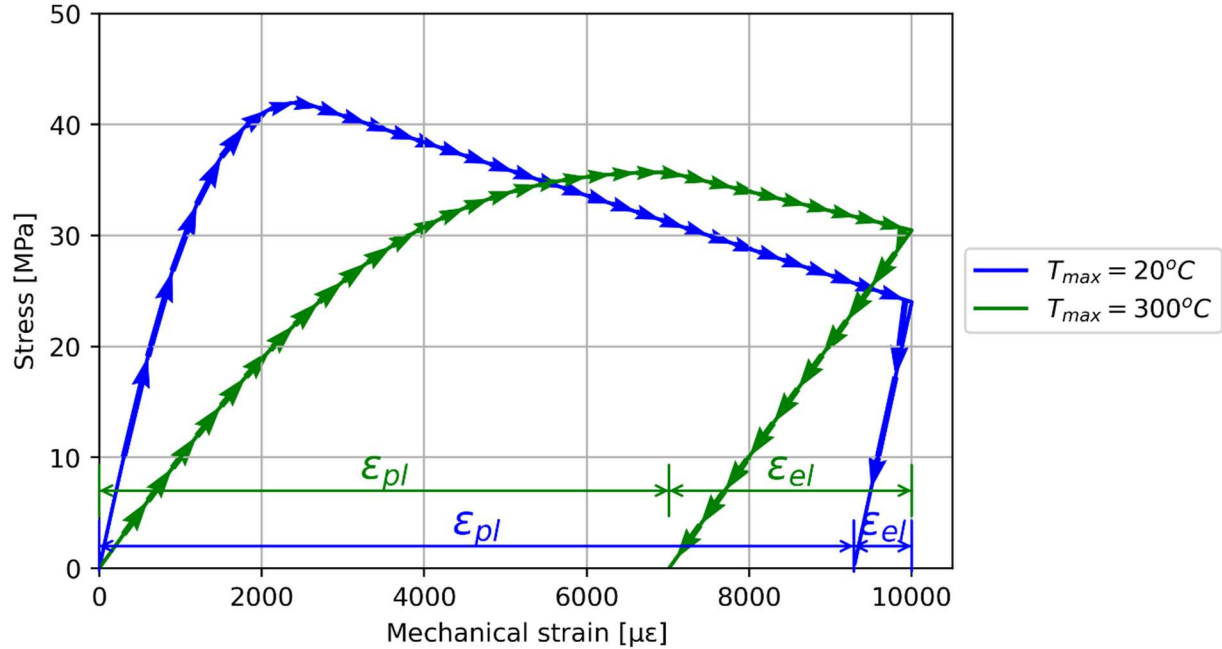


Figure 5. Comparison of the stress-strain diagram of concrete during loading and unloading at ambient temperature and after heating to 300 °C

3.3.4. Transient creep strain

The transient creep strain is implemented in accordance with the model presented in [13]. Transient creep strain is a function of both the temperature and the compressive stress level of the concrete. It is irreversible, meaning that it can only increase with temperature and load. When the concrete temperature decreases, the transient creep strain remains constant.

3.3.5. Strains in reinforcement steel

As for the behaviour of the steel reinforcement, only two strain components are considered: thermal and mechanical. The thermal strains are implemented as per [9] and are fully reversible. Mechanical strains are modelled considering their connection to the stresses. The strain-stress relationship is also defined according to [9] and, similarly, as for the concrete, the distinction between the plastic and elastic strain is done considering an unloading branch with the slope equal to the temperature-dependent modulus of elasticity.

With regard to the post-fire recovery, the following model has been implemented. It is recognized that when steel is heated to temperatures higher than 500 °C, a permanent reduction in its yield strength is observed [14]. This behaviour is modelled using the following relationship in accordance with [15] that defines the yield strength reduction coefficient $k_{res,y}$:

$$k_{res,y}(T_{max}) = \begin{cases} 1, & T_{max} < 500^{\circ}\text{C} \\ 1 - \frac{T_{max} - 500}{1000}, & 500^{\circ}\text{C} \leq T_{max} < 1200^{\circ}\text{C} \end{cases} \quad (8)$$

3.4. Model validation

The model results are compared with data obtained through fire experiments on three concrete beams (C30/37 quality with measured mean compressive strength of 45.7 MPa). Each beam measured 380 cm in length, 20 cm in width, and 29 cm in height. The beams have five longitudinal steel bars (B500, 16 mm diameter with a measured yield strength of 565 MPa). Three bars are positioned in the tension zone and two in the compressed zone, with a cover of 20 mm, resulting in a reinforcement ratio of about 1%. As shear reinforcement, 8mm diameter stirrups spaced 20 cm apart were placed. The design bending moment capacity (M_{Rd}) is 61.6 kNm. The beams were cast with thermocouples inside

them at different depths (12, 20, 50, 100, 150 and 278 mm) that enabled monitoring of the temperatures during heating and cooling.

The beams were subjected to a four-point bending load setup where the load was kept constant resulting in a 41.25 kNm moment in the central zone of 210 cm length throughout the whole duration of the experiments. In a subsection 70 cm in length within this zone, the beams were exposed to radiative heat flux from the tensioned side only, resulting in a one-dimensional heat transfer through the height of the beam. This heat flux was analogous to the EPFC exposure with a time function factor of $\Gamma = 0.45$ and a heating phase lasting 60 minutes. The subsequent cooling phase featured a linear temperature decrease from 826°C at 60 minutes to room temperature at 233 minutes after the test began. (Figure 6). During the tests, deformations in the compressed half of the midspan zone were monitored using Digital Image Correlation (DIC) equipment. This enabled estimating the curvature in this zone. Finally, the residual bending capacity of all beams is conducted through a four-point flexural bending test. A detailed description of the tests is available in [16].

Figure 6 compares the temperatures measured during the test to the ones calculated using the heat transfer analysis. Overall, a good match is observed, even though there is a slight overestimation of the temperatures closer to the heat-exposed surface. It can be concluded that the heat transfer model produces an adequate estimate of the real temperatures inside the concrete beams.

Figure 7 compares the curvature of the heat-exposed constant moment zone in the midspan of the beams as measured during the tests to those numerically obtained using the model. Similarly to the temperatures, the overall match between them is good. There is a slight overestimation of the curvature during the heating phase, which can be traced back to the overestimation of the temperatures during the same phase, most notably the temperature of the reinforcement. During the cooling phase, there is an underestimation of the curvature, which can similarly be attributed to faster cooling observed in the heat transfer results compared to the experimental results. Based on these results it can be concluded that the model for obtaining strains presents a reasonable engineering method of modelling the beam's behaviour during and after the heat exposure.

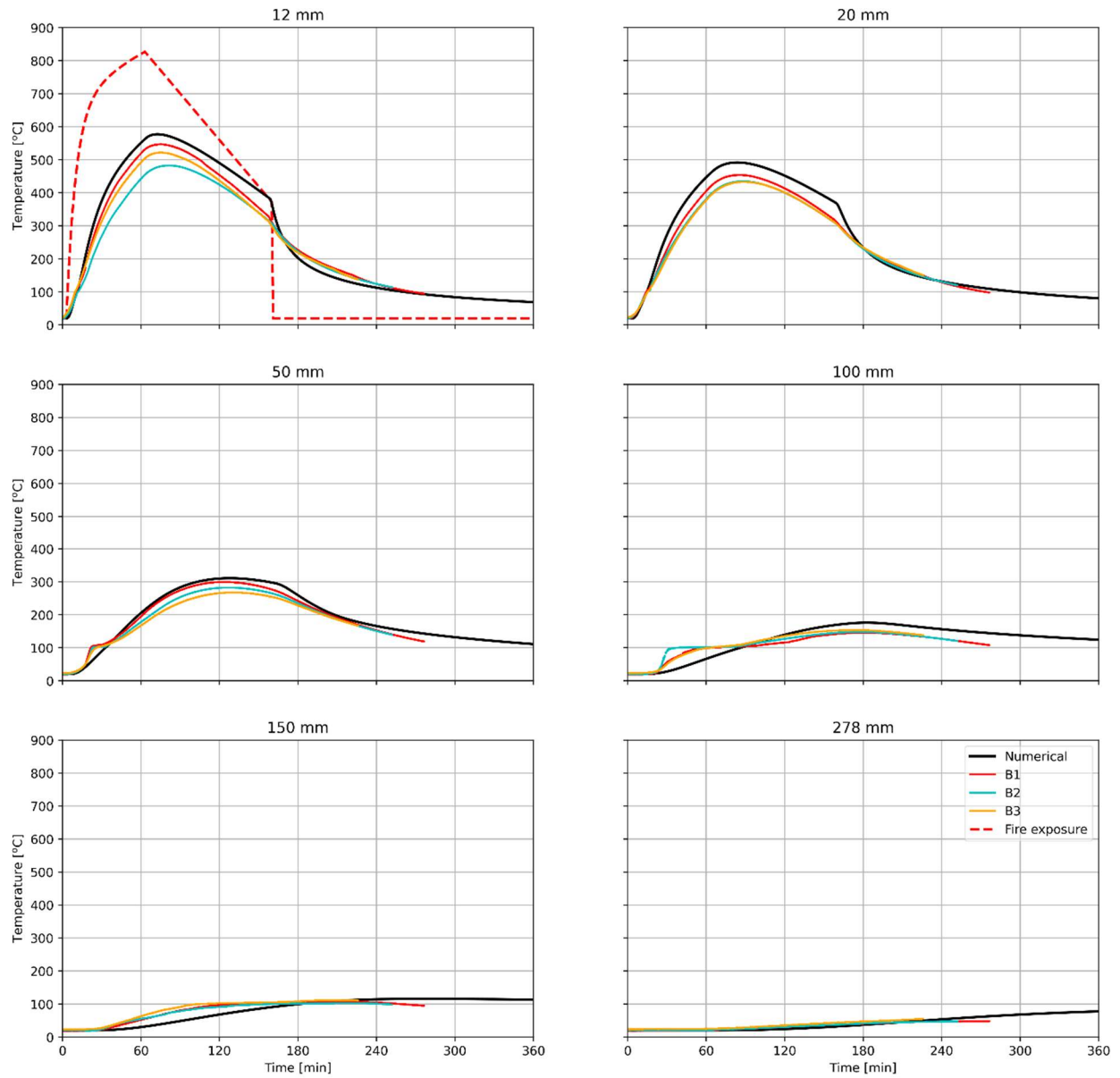


Figure 6. Temperature measured at different depths during the experiments on beams B1, B2 and B3, and obtained numerically using the heat transfer analysis described in Section 3.2.

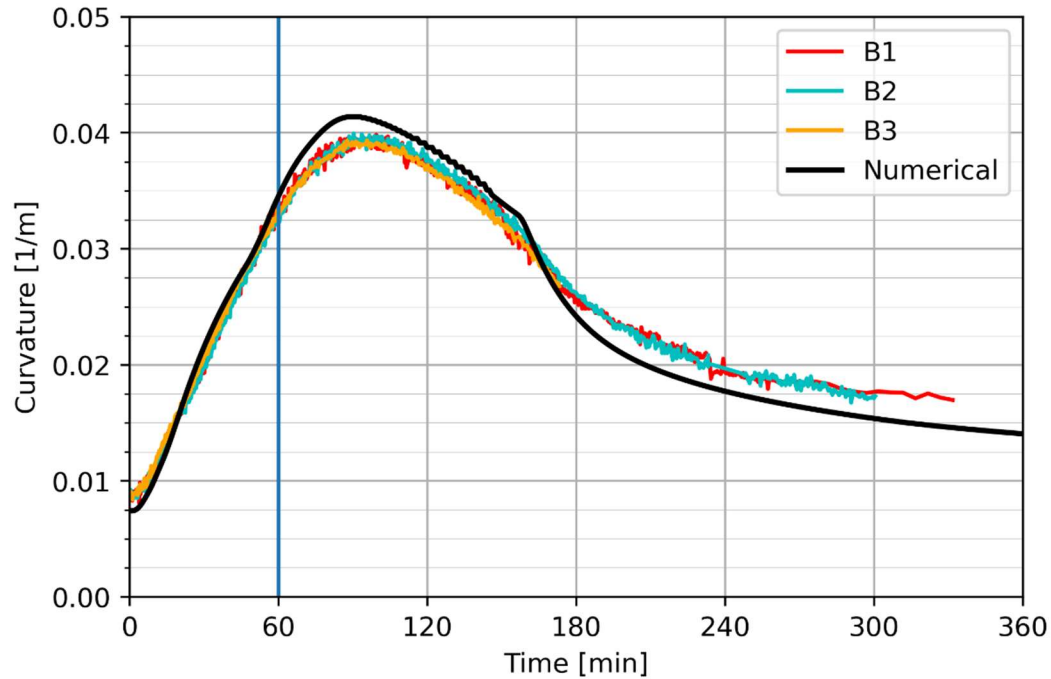


Figure 7. Curvature of the heated midspan zone measured during the experiments for beams B1, B2 and B3, as well as the numerical results of the model described in 3.3.

3.5. Strain distribution

The final result of the model is presented in Figure 8, i.e., the distribution of all of the residual strain components and their sum determined through the numerical model. Plastic strains occur mostly in two zones: close to the top compressed edge and close to the bottom tensioned edge (negative values of the cross-section height represent the heat-exposed half of the beam). The top plastic strains are a consequence of high compression during fire exposure. The bottom plastic strains are the result of large mechanical compressive strains during the fire exposure which result from internal compatibility requirements. A mechanical compression zone forms at the tension side of the beam when the thermal (tension) strains are higher than the total tension strains in that zone.

The residual thermal strains form two zones. In the first zone, the maximum temperature did not exceed 430 °C and the residual strains are compressive (i.e., residual shrinkage). The second zone, concentrated near the fire-exposed edge, has high-tension residual strains (i.e., residual expansion).

Two similar zones as in the case of the plastic strains can be seen in the transient creep strain distributions. This is expected as both are a consequence of large compressive effects. However, it can be noticed that the transient creep strains are much higher near the fire-exposed edge due to the higher temperatures in that zone.

Particularly noteworthy are the residual strains in the top, compressive, zone. This demonstrates again that the effect of fire is not localized near the exposed surface, but affects the entire cross-section. These residual strains will have an effect on the position of the neutral axis for cases when the loading is relatively low.

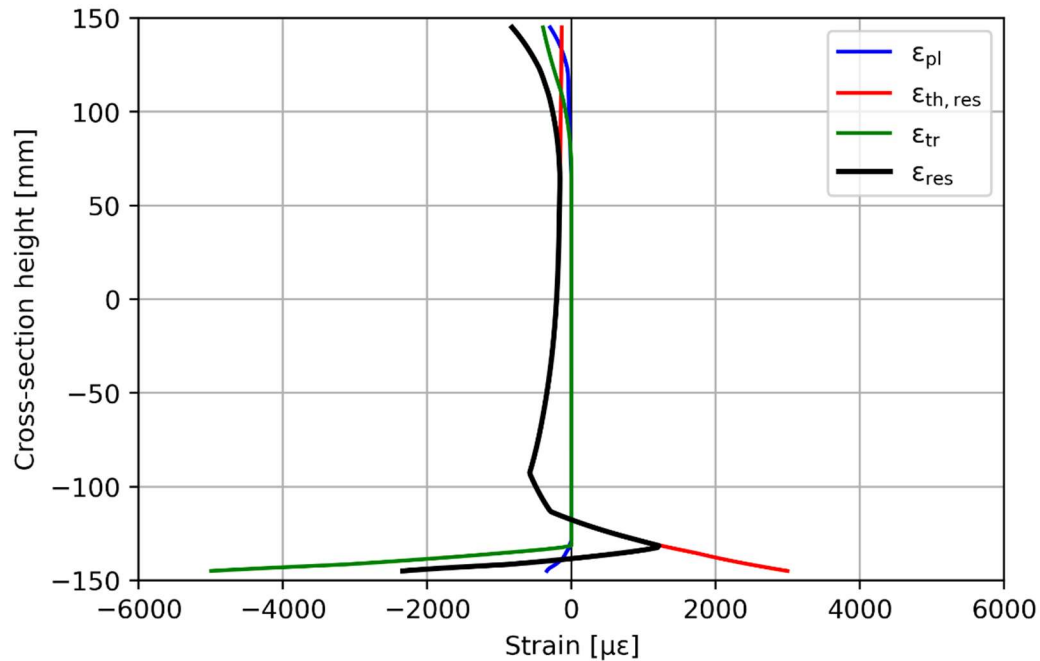


Figure 8. Residual strain component distributions at the end of the heating and cooling phase based on the model (negative values of the cross-section height represent the heat exposed half of the beam)

3.6. Neutral axis position

Once all the residual strains have been determined numerically for any value of the applied moment to the cross-section post-fire, the total strain distribution can be easily calculated. Using Eq. (4) the position of the incremental neutral axis similar to the one that can be measured by the FBGs can be calculated. This is done by calculating the changes of the curvature and strain at the centre of the cross-section (based on the total strain distribution) for small changes in the applied moment. The outcome of such calculation is illustrated in Figure 10 where the position of the neutral axis for any value of applied moment on the cross-section is shown for the case of the beams from the experimental campaign. The figure shows results calculated by the numerical model for two cases: using the residual strains before the fire exposure and using the residual strains after it. The positive moments represent cases when the fire-exposed side is in tension as shown in Figure 9

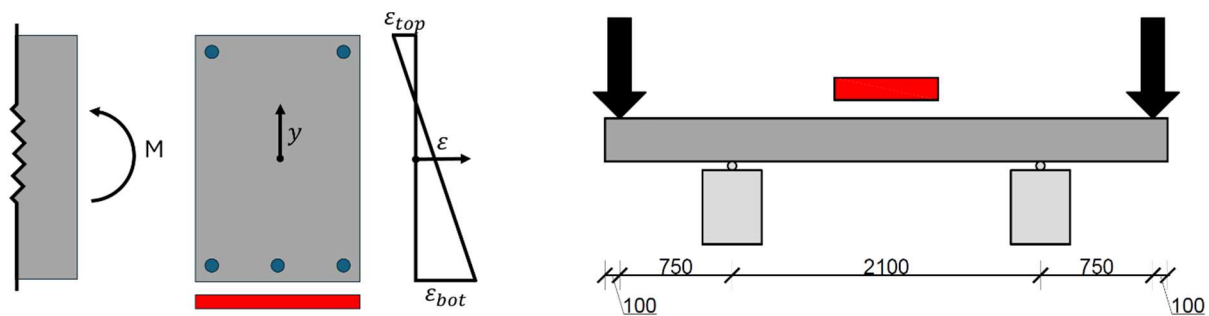


Figure 9. Schematic description of the beam cross-section and used coordinate system for the position of the neutral axis together with the setup configuration during the test (red colour represents the edge exposed to the heating)

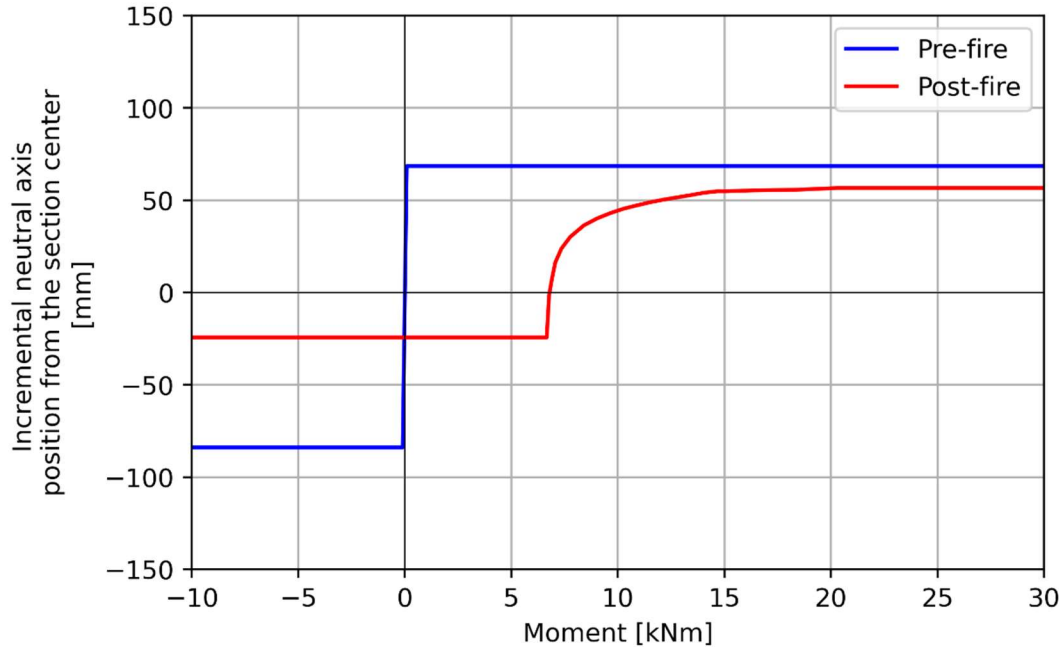
Figure 10 shows the resulting incremental neutral axis in both pre- and post-fire conditions as a function of the total applied moment on the cross-section (i.e. including self-weight). In the pre-fire = case (blue), the beam has damage

(cracks) and residual plastic strains from the applied load of 41.25 kNm only. Two distinctive zones can be seen, when the moments are positive, the position of the neutral axis is 68.5 mm while for negative moments it is -85.1 mm. The presence of two distinct values can be attributed to the inherent asymmetrical behaviour of concrete when subjected to tension and compression and the asymmetric placement of reinforcement. Under low-stress conditions, concrete exhibits symmetrical behaviour in tension and compression; however, its tensile strength is significantly lower than its compressive strength. Consequently, the reinforcement bears most of the tensile stresses, while concrete is predominantly exposed to compressive stresses. This leads to a shift in the neutral axis towards the side that is compressed. The larger magnitude of the negative moment (85.1 vs 68.5 mm) can be attributed to the lower reinforcement area in the top zone (2 vs 3 bars).

In the post-fire case, three distinctive zones are observed. For larger positive moments the position of the neutral axis is constant at 55.7 mm. In the second zone of mostly negative moments, the neutral axis position is constant at 23.4 mm. The observation that the neutral axis position remains negative also for small positive moments post-fire can be explained by considering that the total strains in concrete post-fire are a sum of two parts: residual strains, i.e., permanent deformations remaining after the fire exposure, and elastic strains, which will influence the stress level in the concrete. If, in the upper part of the structure, the total compressive strains are smaller than the residual compressive strains (this holds true for small positive moments) then the elastic strains in that area will be tensile in order to compensate for the large residual strains. Depending on the magnitude of these tensile strains, and taking into account that most of the cross-section is cracked post-fire, the contribution of concrete to the internal forces may become insignificant in case of small external loads. Consequently, the neutral axis position remains fixed at -23.4 mm, which aligns with the centre of gravity of both top and bottom reinforcement. These observations highlight the complex behaviour of concrete structures after exposure to fire, emphasizing the significance of comprehending the interplay between residual strains, concrete cracking, and internal forces.

The third zone is an extensive transition zone between the positive and negative neutral axis results. Such a transition zone exists also in the pre-fire case, but it is concentrated around values where the moment is almost equal to zero and is very small. The bigger prominence and position of this transition zone in the post-fire case can be explained by considering two factors: residual strains and concrete cracking. Due to the fire exposure, cracking predominantly occurs within most of the cross-section, leading to a complete loss of tensile strength of concrete within these regions. Additionally, the exposure to elevated temperatures resulted in significant residual compressive strains within the top compression zone of the beam (Figure 8). These effects are the same as discussed above to explain the negative neutral axis position (second zone) for small bending moments. However, in this transition zone, one part of the elastic strains in this area becomes compressive. This can be seen in Figure 11, where the elastic strain distribution is presented. To elaborate, when all the elastic strains in the top zone are positive (tensile) the position of the neutral axis is negative. As the moment increases, some of these strains become negative (compressive), coinciding with the shift in the neutral axis position. This marked transition zone results from the significant nonlinear effects which result in the concrete only gradually contributing to the overall equilibrium of the cross-section, moving the neutral axis from the reinforcement centre of gravity towards the top concrete compressive zone. Unlike the pre-fire case, the presence of residual strains shifts the transition zone to higher applied moment values and, due to the highly nonlinear nature of these strains, makes the transition broader and nonlinear.

In the remainder of this paper, the converged “zone 1” neutral axis position will be reported since the beam is considered to be loaded with significant positive bending moment in real conditions.



on

Figure 10. Post-fire position of the incremental neutral axis calculated for the beams from the experimental campaign

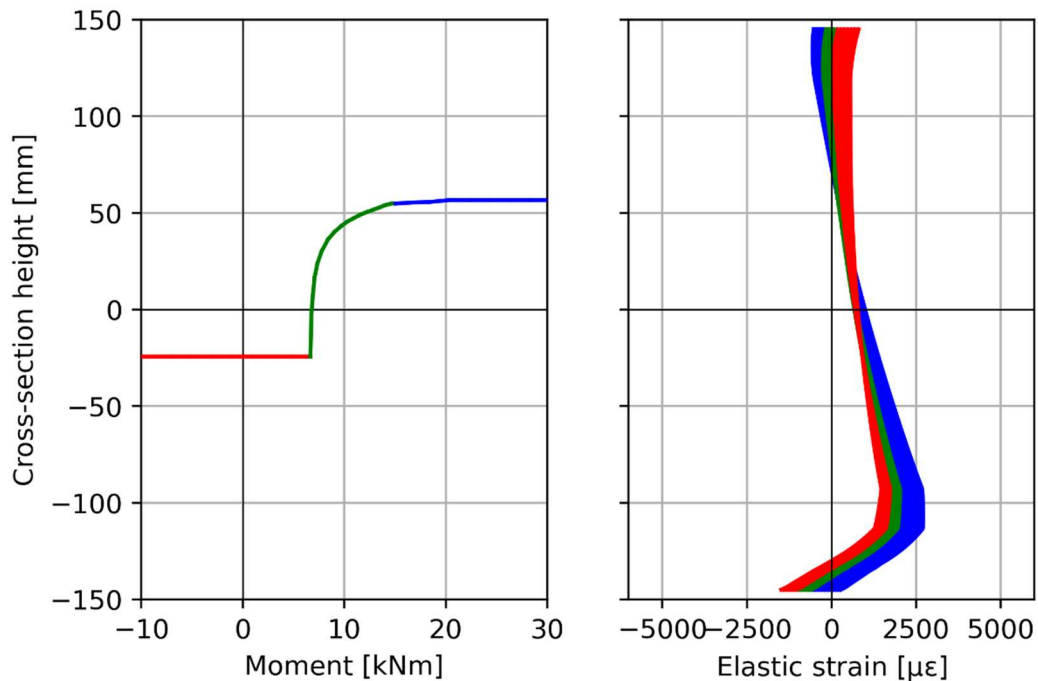


Figure 11. Post-fire elastic strain distribution through the cross-section height in the function of the applied moment (zone 1 – blue, zone 2 – red, zone 3 – green),

In order to clarify how the position of the neutral axis is influenced by different parameters (opening factor O , fuel load q_f , concrete compressive strength f_c and reinforcement yield strength f_y), the results of a parametric study are presented in Figure 12, considering an applied moment of 41.25 kNm (i.e., zone 1 for the neutral axis position). In each graph, one parameter was varied in addition to the fuel load while others remained constant at values: $O =$

$0.1 \text{ m}^{1/2}$, $f_c = 42.9 \text{ MPa}$ and $f_y = 560 \text{ MPa}$ (in the case of the fuel load graph, the second varied parameter is concrete compressive strength). For the considered input values, all EPFC exposures are ventilation controlled and for the combination of the parameters where the beam does not survive the fire, the value of the neutral axis has been omitted. First, it can be observed that each parameter has a substantial influence on the position of the neutral axis, with fuel load and compressive strength having the biggest effect. The neutral axis position is not very sensitive to the opening factor and the reinforcement yield stress when the fire exposure is less intense (low fuel load), but they influence the neutral axis position more for more intense fires. Another interesting observation is that the neutral axis shifts to more positive values (away from the tensioned fire-exposed edge) with a decrease in the fire intensity (higher O and lower q_f). This suggests that for a lower level of fire damage, the neutral axis has higher values. Furthermore, this shift to more positive values is also seen for an increase in the mechanical properties, suggesting that beams that have a higher capacity pre-fire will experience a bigger shift of the neutral axis. This is in contrast with the behaviour observed for prestressed beams damaged by bending cracks [5]. The results of the parametric study highlight the complex behaviour of the neutral axis position in the case of fire exposure and underline the need for the complex strain analysis in determining its position as presented above.

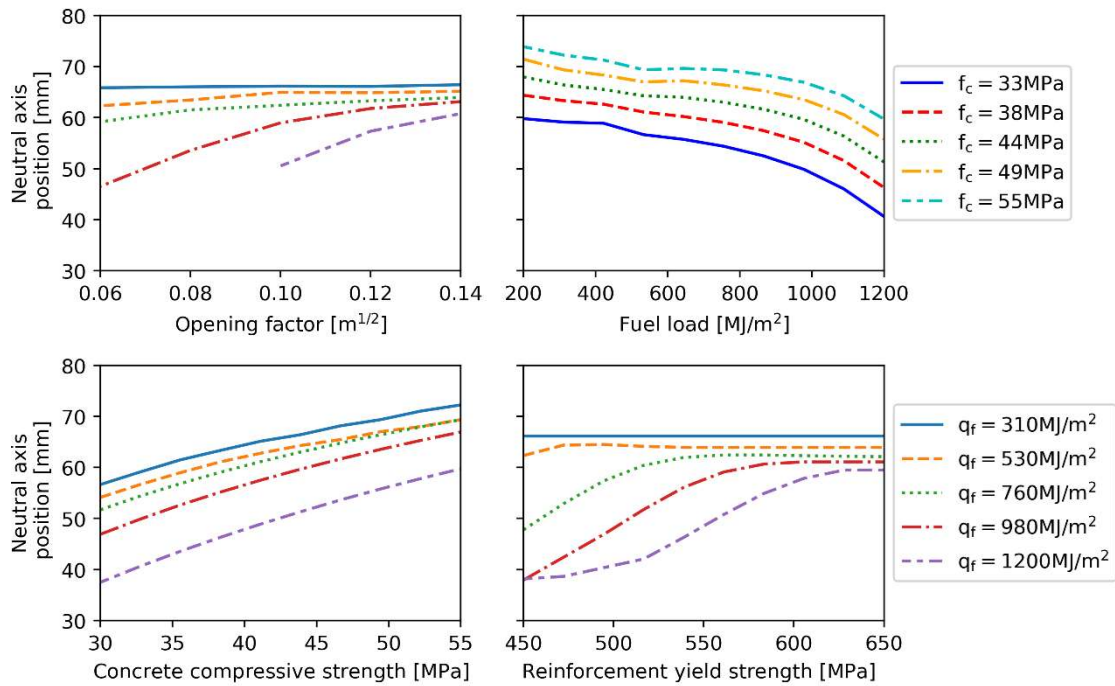


Figure 12. Neutral axis position in function of the input parameters. For each graph one parameter and the fuel load are varied while others stay constant: $O = 0.1 \text{ m}^{1/2}$, $f_c = 42.9 \text{ MPa}$ and $f_y = 560 \text{ MPa}$ (in the case of the fuel load, the second varied parameter is the concrete compressive strength).

4. Bayesian updating framework

4.1. Concept

As a statistical inference technique, the Bayesian approach accounts for uncertainties and errors by updating a probability distribution of the parameters of interest [17]. Applied to the case at hand, this produces updated distributions of the parameters that define the fire exposure and material properties of the beam on the basis of FBG measurements after the fire. Using these updated probability distributions as inputs for further calculations, an updated assessment of the beam's residual capacity can be obtained.

In section 3 above, a model has been presented that allows for the evaluation of the position of the incremental neutral axis. This model allows assessment of the measured quantities (neutral axis position) for given values of the

parameters of interest (fire exposure and material parameters), and is therefore called a “forward model”. The forward model thus enables the use of Bayesian updating to obtain an updated assessment of the parameters of interest given an actual measurement of the neutral axis (i.e. by the FBG measurements). The methodology presented here will be further elaborated considering four parameters: two that influence the fire exposure (opening factor during the fire O and fuel load consumed during the fire q_f) and two parameters that define the material properties of the beam (the compressive strength of concrete f_c and reinforcement yield stress f_y , both at initial ambient conditions). It should be noted that the bending stiffness of the beam, a very important parameter, is implicitly taken into account through these parameters as they will uniquely define the stiffness associated with the temperature-dependent material models introduced in Section 3.3. More precisely, the modulus of elasticity of concrete is defined based on the stress-strain diagram presented in Section 3.3.3, which states that it is a function of f_c and temperature it experienced. All the other parameters needed for the model, such as the compartment geometry and characteristics, beam geometry and loading are not considered to be uncertain as they can be readily assessed with reasonable accuracy post-fire.

The methodology is schematically represented in *Figure 13*. Each step in the methodology is presented in the following text.

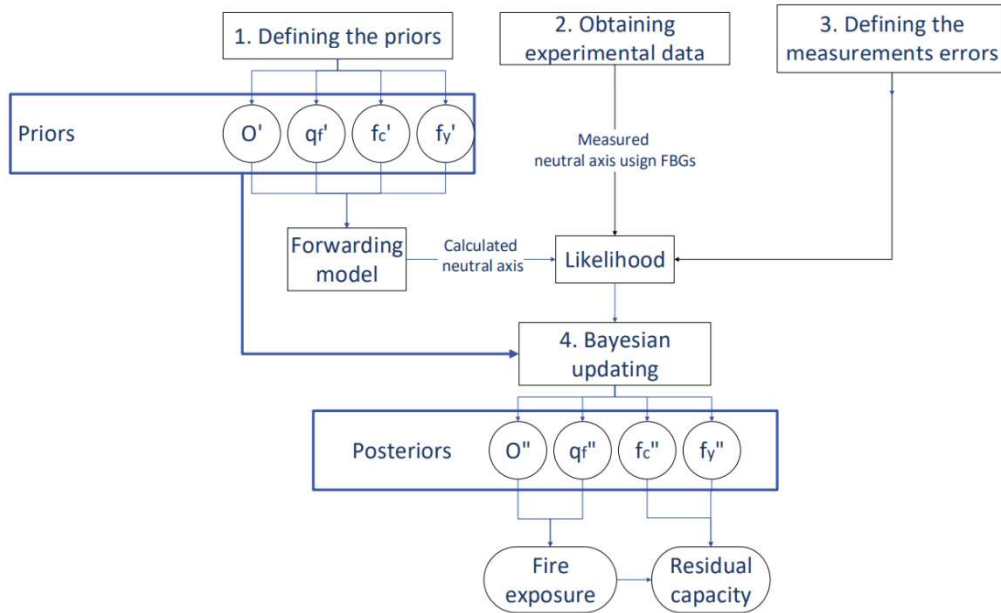


Figure 13. Schematic representation of the Bayesian methodology employing the neutral axis position for the post-fire assessment

In order to update the prior distributions of the four parameters of interest, the errors associated with the measured maximum temperature and depth need to be assessed. When they are assessed, two components must be taken into account: the measurement error and the modelling error (i.e., the error within the forwarding model). When there is only limited information on the different error components, it is advised to consider the total error as the sum of the components (Eq. (9)) [18]. In this case, the error is modelled as unbiased and normally distributed.

$$\varepsilon_{total} = \varepsilon_{measurement} + \varepsilon_{modeling} \quad (9)$$

The updating is achieved by applying Bayes' theorem, which relates the probability density function of the parameters given the data f'' to the probability of the data given the parameters (the likelihood) L and the parameters' prior probability density function f' . This is presented in Eq. (10):

$$f''(q_f, O, f_c, f_y | NA) \sim L(NA | (q_f, O, f_c, f_y)) \cdot f'(q_f, O, f_c, f_y) \quad (10)$$

The likelihood is calculated using the following formula,

$$L = (2\pi\sigma_{NA})^{-\frac{1}{2}} \exp\left(-\frac{(NA - M_{NA})^2}{2\sigma_{NA}^2}\right) \quad (11)$$

where σ_{NA} is a standard deviation of the normally distributed error for the position of the neutral axis and M_{NA} is the model results for given inputs determined as explained in section 3. This equation considers that the error is unbiased and normally distributed ($\varepsilon_{NA} \sim N(0, \sigma_{NA})$).

Using this expression for the likelihood, updating can be performed and samples from the posterior distribution can be obtained utilizing the Markov Chain Monte Carlo (MCMC) method with the Metropolis algorithm, explained in detail in [17]. The MCMC samples the posterior distribution using a rejection algorithm for sampled sets of q_f , O , f_c and f_y from the posterior distributions. For each sample, a realization of the forwarding model is obtained in order to calculate the likelihood. As this is highly computationally expensive, a surrogate model is used for determining the neutral axis position. Specifically, it is a quadratic interpolation surface based on 10^4 model evaluations chosen using Latin hypercube sampling. Therefore, σ_{NA} should account for the additional error introduced by the surrogate model by adjusting the modelling error in Eq. (9).

Based on the obtained posterior distributions for q_f and O , and the adopted model of the EPFC, maximum temperatures inside the member and associated reduction of material strength can be estimated, allowing to determine the residual capacity of the structure. This is illustrated further in Section 5.

5. Demonstration

5.1. Case description

In order to validate the methodology, results from the previously mentioned testing campaign are used. Neutral axis position obtained using quasi-static tests is used. In these tests, the beams were positioned in a 4-point bending setup, where the supports were positioned 10 cm from the edges and the load application points were spaced 120 cm from the supports. This formed a 120 cm long zone with the constant moment where the tension was on the bottom of the beam. In order to monitor the strains, two chains of FGB strain sensors were attached to the top and bottom at one side of the beams (2.5 cm from the edges). The loading on the beam was gradually increased until the moment of 30 kNm in the midspan (25 kN force at both application points) and then decreased back to zero while the FBG sensors were used to monitor the strains. The position of the neutral axis is determined based on the change in the strain values when the loading level changes. An increment of 1 kN of the applied force was used. This is equivalent to the small changes in curvature that occur when the beam vibrates and provides the position of the neutral axis similar to the one measured using the vibration technique at different load levels. The results for the midspan sections of all beams are presented in Figure 14. Based on the results for higher load levels, the positions of the neutral axis are 50.4 mm, 55.1 mm and 57.5 mm for beams B1, B2 and B3 respectively, which had identical dimensions and material used and were exposed to the same heating exposure.

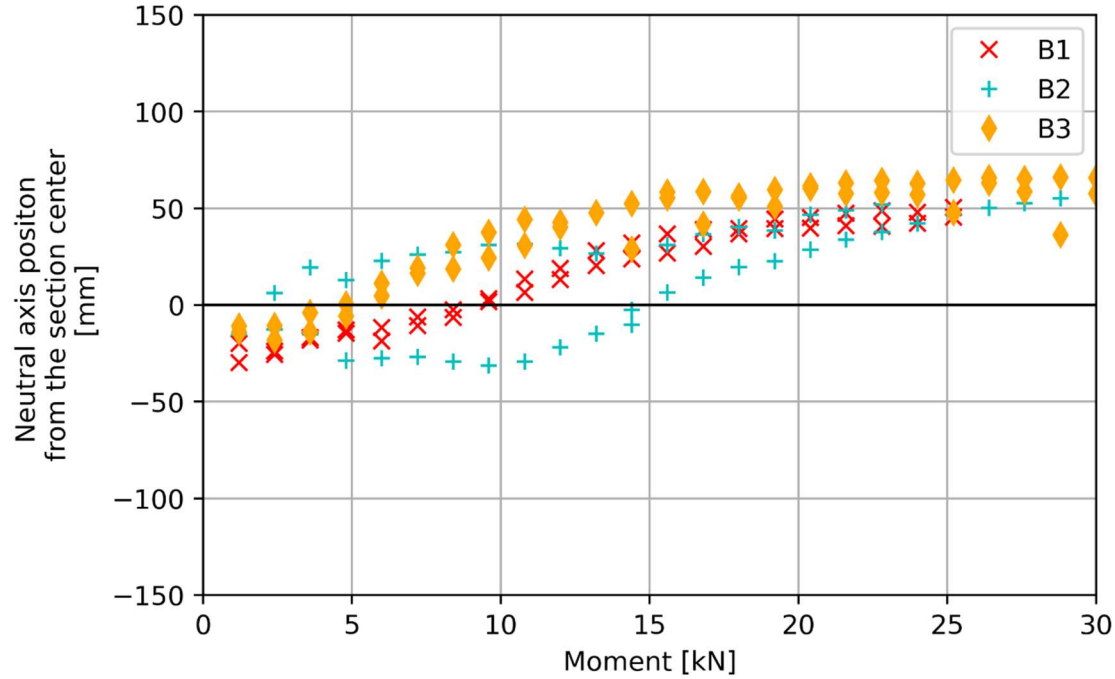


Figure 14. Incremental neutral axis positions at midspan during four-point load testing, obtained from static strain increments corresponding to load increments ΔF of 1 kN: experimental values

5.2. Prior distributions

The data obtained from the quasi-static tests is used to conduct Bayesian updating in order to determine the residual behaviour of the beams after the heating exposure. The first step is defining the prior distributions of the parameters that are going to be updated. In the real-life scenario, these distributions would be determined based on the compartment geometry and characteristics and beam characteristics. For the material properties, these distributions are determined based on the class of the materials used, i.e. concrete C30/37 and reinforcing steel B500. However, as the heat exposure was artificial, the prior distributions are chosen to be in line with real-life situations. The prior distribution for the fuel load is chosen according to EN 1991-1-2 [9] for dwellings. The heat exposure applied during the tests mimicked the effects of an EPFC with a factor $\Gamma = 0.45$ and a heating duration of 60 min. This corresponds to the EPFC obtained with opening factor $O = 0.033 \text{ m}^{1/2}$, fuel load $q_f = 565 \text{ MJ/m}^2$ for a $10 \text{ m} \times 10 \text{ m} \times 3 \text{ m}$ compartment whose linings have thermal inertia of $b = 1450 \text{ J/m}^2 \text{ Ks}^{1/2}$. For that reason, for the opening factor a prior distribution according to [19] ($O = O_{\max}(1 - \xi)$) with the maximum opening factor of $O_{\max} = 0.04 \text{ m}^{1/2}$ is used. The parameter values of the considered prior distributions are presented in Table 1.

Table 1 Prior distributions used in the case study

Value	Unit	Distribution	Mean	St. Dev.
Parameter ξ	-	Truncated Lognormal	0.2	0.2
Fuel load q_f	MJ/m^2	Gumbel	780	234
Concrete compressive strength - f_c	MPa	Lognormal	42.9	6.4
Steel yield strength - f_y	MPa	Lognormal	560	30

5.3. Bayesian updating results

The measurement error magnitude was assessed numerically based on Eq (1). The neutral axis position is obtained by measuring the values of the top and bottom strains and the positions of the sensors on the beam. The strain error is assumed to be equal to 1% according to [5] and the error of the position measurements is assumed to be equal to 1

mm based on the measuring equipment used to measure their position. Using this information, Monte Carlo simulations are conducted and an error equal to 1.6 mm is obtained. To include the error of the forward model, a value of $\sigma_{NA} = 2$ mm is implemented.

The Bayesian updating process was carried out using the MCMC (Markov Chain Monte Carlo) method and the Metropolis-Hastings algorithm to sample the posterior distribution. Four distinct chains each consisting of 10^5 samples were generated. The proposal distribution was chosen as a Normal distribution with a constant coefficient of variation of 0.1 for each parameter. This resulted in an acceptance ratio of approximately 0.4 for all chains. A visual inspection was employed to determine the burn-in period, discarding the initial 20% of samples that had not yet converged to the posterior distribution. As a result, 3.2×10^5 samples remained for the updated parameter values.

The outcomes of the parameter update are presented in Figure 15 to Figure 18. Figure 15 depicts the updated result for the opening factor during the fire. It is noteworthy that there is no substantial reduction in the uncertainty associated with this parameter, indicating a low sensitivity of the neutral axis position to this factor. A similar observation can be made for the reinforcement yield strength shown in Figure 18.

In Figure 16, the update results for the fuel load display the most significant reduction in variance. The coefficient of variation (COV), was reduced from 0.3 for the prior distribution to 0.15-0.17 for the posterior distribution. Moreover, the posterior distribution's most likely value is close to the actual value for all three beams. Finally, for the compressive strength of concrete, shown in Figure 17, also a significant reduction of variance is observed, from prior 0.15 to posterior 0.09-0.11. However, three distinctive most likely values for each beam can be seen: the lowest one for beam B1 with the lowest value of the neutral axis position; the highest for beam B3 which had the highest measured position of the neutral axis and beam B2 sitting in the middle for both categories. The subsequent step involves analyzing the impact of these updated parameters.

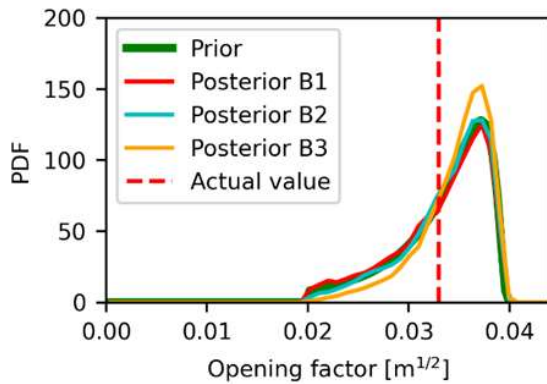


Figure 15. Prior and posterior distributions for the opening factor

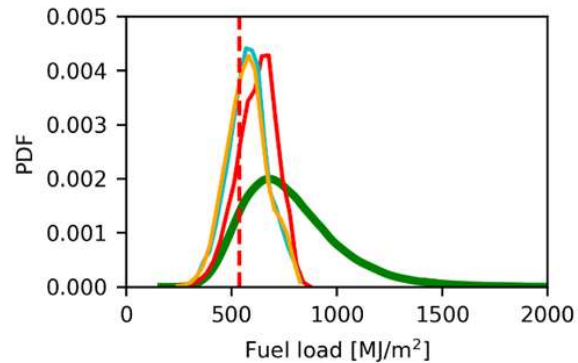


Figure 16. Prior and posterior distributions for the fuel load

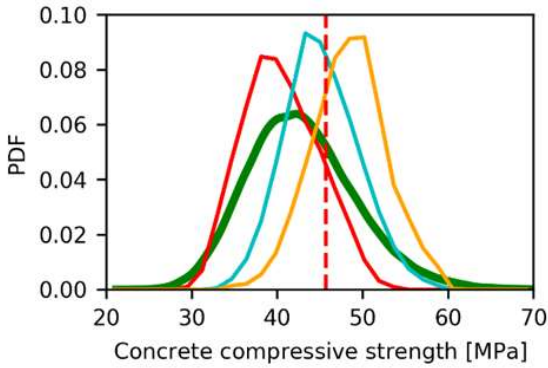


Figure 17. Prior and posterior distributions for the concrete compressive strength

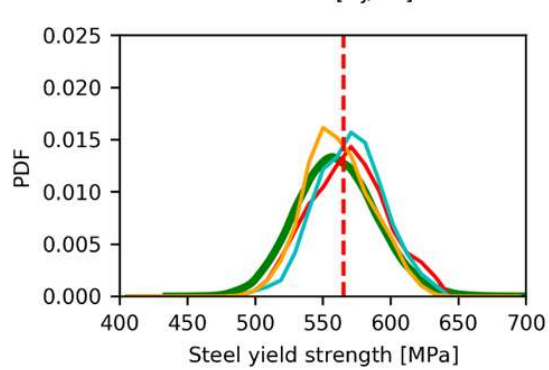


Figure 18. Prior and posterior distributions for the reinforcement yield strength

Using the updated values of the opening factor and the fuel load for beam B2, the posterior assessments presented in Figure 19 are obtained. The top left graph presents the temperature-time curve, with the 95% highest density interval depicted as a shaded area. Notably, the posterior interval (represented in red) is narrower compared to the prior distribution (shown in green). The posterior distribution is observed to be concentrated closely around the actual fire curve (indicated by the red dashed line). This visualization highlights the significant reduction in the range of potential fire scenarios following the update process. Similar results are seen for beams B1 and B3.

The maximum temperature profile, usually the prime interest of post-fire assessment [20], [21], is shown in the top right graph. Similarly, it is evident that the posterior temperature profile exhibits a narrower range which aligns closely with the actual temperature observations. The same trend of increased precision can be observed in the bottom right graph, which displays the residual concrete strength profile. The posterior distribution demonstrates a noticeable narrowing down of possible strength reduction scenarios, with a more concentrated range of values around the true residual concrete strength profile. Lastly, the bottom left graph shows the distributions of the damaged layer thickness. This measurement refers to the depth at which the residual strength is equal to 80% of the initial strength. This depth is equal to the position of the 350 °C isotherm of the maximum temperature gradient, as, according to the adopted model of EN 1994-1-2:2005 residual strength for that temperature is equal to 80% of the original one). These visual representations provide a tool for further analysis and understanding of the effects of fire on structural elements, enabling engineers and researchers to make informed decisions for post-fire assessment and mitigation strategies.

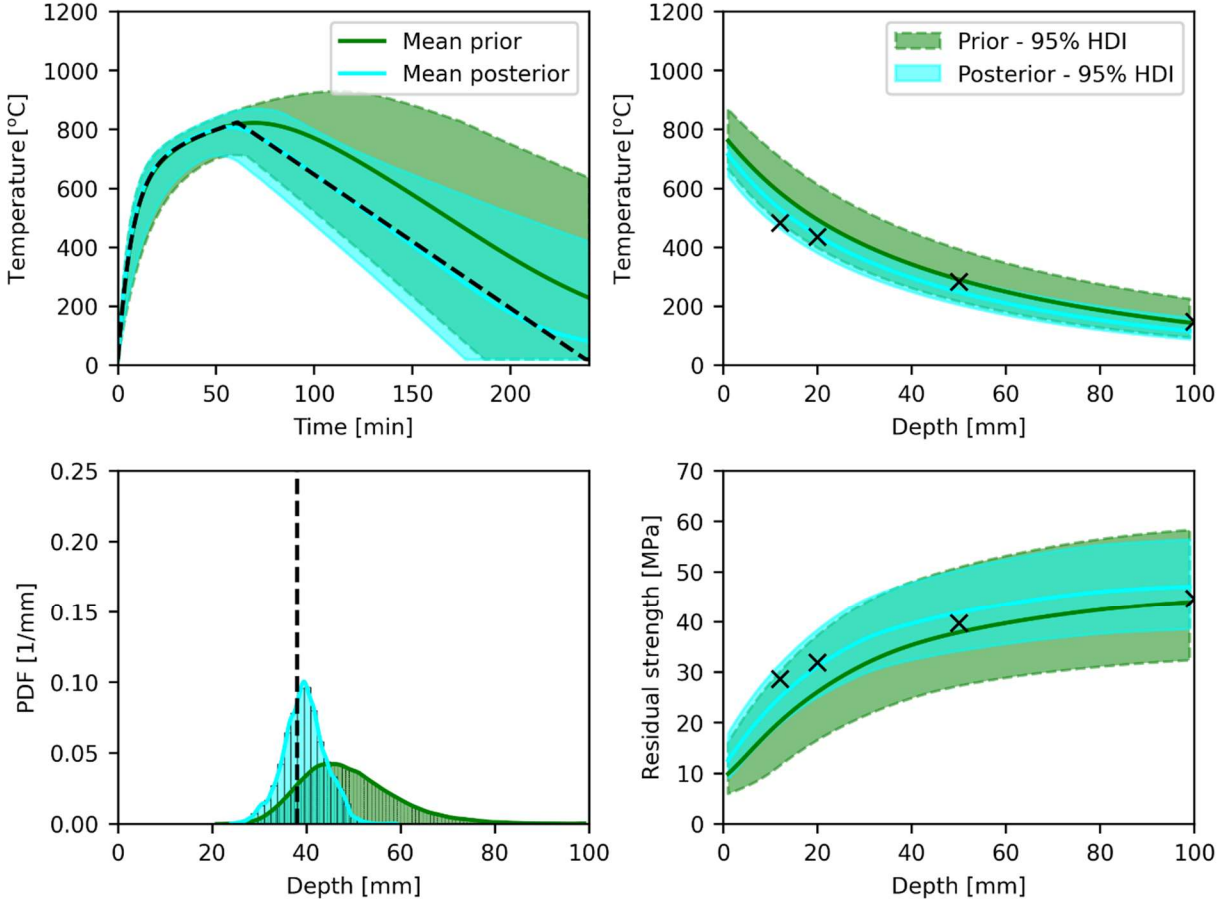


Figure 19. Results of the Bayesian update – Fire exposure (top left), Maximum temperature profile (top right), Residual compressive strength (bottom right) and Damage layer depth (bottom left); The shaded area represents the 95% highest posterior density interval for prior (green) and posterior (cyan) distributions; black dashed lines and points are the true reference values.

5.4. Residual bending capacity

Utilizing the updated data, an assessment can be made regarding the residual post-fire bending capacity of the beam. This capacity can be determined through the application of the following formula [22]:

$$M_R = k_{y,res} \cdot f_y \cdot A_s \cdot \left(h - c - \frac{\Phi}{2} \right) - \frac{(k_{y,res} \cdot f_y \cdot A_s)^2}{2 \cdot b \cdot f_c} \quad (12)$$

where f_y is the yield strength of the reinforcement steel, A_s is the reinforcement area, h is the beam height, c is the concrete cover, Φ is the reinforcement bar diameter, f_c is the concrete compression strength at ambient conditions (under the assumption that the concrete in the top compression zone did not reach high temperatures), b is the beam width and $k_{y,res}$ is the residual strength retention factor of the reinforcement after heating.

To obtain the residual strength retention factor, the maximum temperature profile within the concrete, as derived from the Bayesian analysis, can be employed. The factor $k_{y,res}$ is obtained based on the reinforcement temperature and Eq. (8).

where T_{\max} represents the maximum temperature the reinforcement has experienced during the heat exposure calculated using the posterior distributions of the opening factor and fuel load. Incorporating this posterior information

along with the posterior distributions of material properties and values for all other parameters listed in Table 2, enables a probabilistic evaluation of the residual post-fire bending capacity of the beam. The geometric values are deterministic and based on the measurements of the beams. The concrete cover was measured after the capacity tests and was equal to the intended 20 mm for all three beams. The concrete compressive strength and reinforcement yield strength are included as stochastic values based on the posterior distributions.

Table 2 Parameters used for obtaining the residual bending capacity of the beam

Name	Unit	Distribution	Mean	Standard deviation
Beam height - h	mm	Deterministic	290	-
Beam width - b	mm	Deterministic	200	-
Concrete cover - c	mm	Deterministic	20	-
Reinforcement diameter	mm	Deterministic	16	-
Reinforcement area - A_s	mm ²	Deterministic	603	-

The results of the update are presented in Figure 20. It is obvious that the posterior distributions shift to the capacity of the beam BR, which is a reference beam that was not exposed to the heating and used to assess the pre-fire bending capacity. It is suspected that the biggest reason for this is the inadequacy of Eq. (8) to represent the actual reduction of the reinforcement strength that occurred during the tests. During the heat exposure, the reinforcement temperature did not exceed 500° C in any of the tests, therefore, according to Eq. (8), the residual capacity should be the same for all three beams. However, the heat-exposed beams show a 7% reduction in the residual capacity. In order to confirm part of this hypothesis, the reinforcement temperature distributions are plotted in Figure 21. A good match is observed for all three beams, suggesting that the updating procedure can infer the reinforcement temperature and that the biggest influence in overestimating the residual capacity is the relationship between the temperature and residual yield strength.

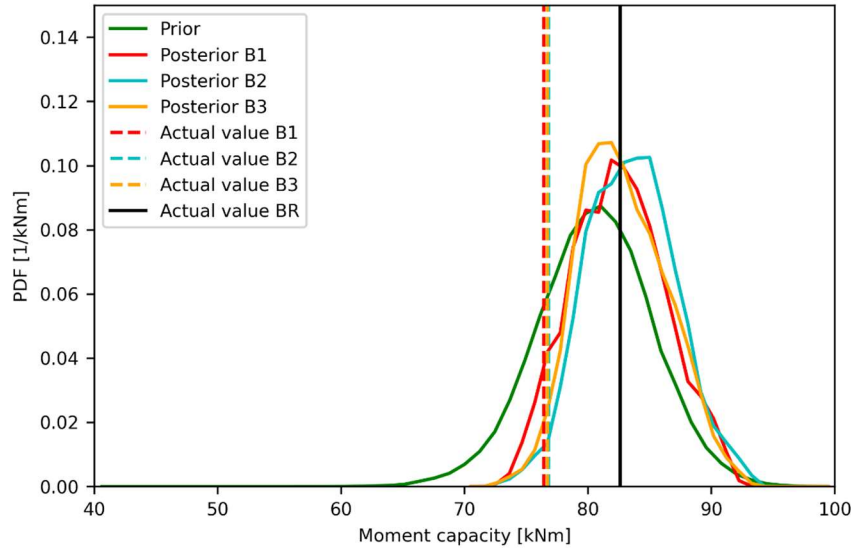


Figure 20. Residual bending capacity distributions based on the prior and posterior distributions

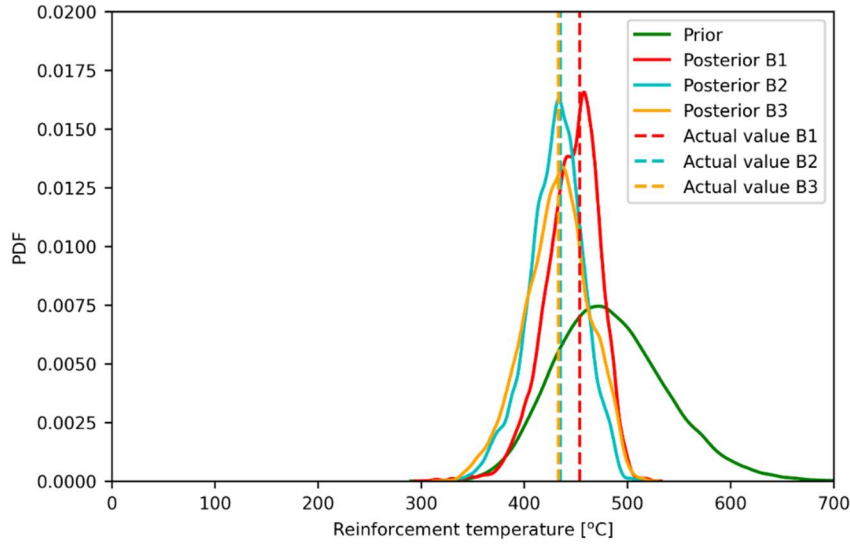


Figure 21. Tension reinforcement maximum temperature distributions based on the prior and posterior distributions

6. Conclusions

A novel methodology for evaluating the post-fire condition of concrete infrastructures has been introduced and analyzed. This methodology employs Fiber Bragg Grating (FBG) sensors to measure macro-strains induced by small member deformations, serving as a non-destructive approach to assess the condition of concrete elements after fire exposure. The core of this technique lies in measuring changes in strain within concrete components under minor deformations and presented in the form of the position of the neutral axis. These strain measurements are significantly affected by the distribution of residual strains across the cross-section, which in turn, are a consequence of both the high temperatures and the mechanical loads encountered during a fire event. In order to properly analyse these relationships, a computational model has been developed that determines the position of the neutral axis as a function of the parameters governing the fire exposure and material properties.

The model has uncovered that the position of the incremental neutral axis is dependent on the loading of the beam during the measurement. In the presented case of a simply supported beam subject to bending, three different zones in the function of the applied moment were seen: a zone where the neutral axis is in the bottom half, a zone where it is in the top half and a transitional zone. Prior to fire exposure, the transition zone was very narrow and concentrated around the moment equal to zero. After the fire exposure, this transition zone is much wider and located around positive moments. Therefore, the loading level during the measurements must be sufficiently high in order to ensure that the measured neutral axis relates to the stable value in the top half of the beam in order to maximise the information obtained using this technique.

It was revealed that the position of the neutral axis moves closer to the centroid when the fire exposure, and therefore the fire-induced damage, is more intense. This highlights the strong effect of the residual strains accruing in the concrete due to the fire exposure and the great importance of modelling them properly.

Due to the nature of the proposed measurement technique, it was employed in combination with Bayesian inference. This ensures that the uncertainties associated with the application of the technique are properly treated and allows for assessing how much information the technique provides. The Bayesian update process enables a more accurate estimation of the parameters of interest.

The effectiveness of the proposed technique has been presented using experimental results, which serve to illustrate the updating process of posterior distributions for parameters defining both fire exposure scenarios and material properties. This demonstration highlights the method's ability to update these parameters, thereby reducing associated uncertainties. It was observed that the technique mostly provides information on the fuel load consumed during the

fire and the compressive strength of the concrete, and only limited information on the opening factor and reinforcement yield strength for the case study treated. The updated maximum temperature values and material strengths obtained through this methodology are instrumental in evaluating the residual structural capacity of the components in question, as well as informing decisions regarding their potential continued use or repair.

The case study shows that the FBG sensors have the potential to be used in post-fire assessment since the measured position of the neutral axis provides important information that can later be used to infer the residual condition of the concrete member after the post-fire exposure. However, in order to provide useful results that also recognize the uncertainty in the measurement and modelling, it should be combined with Bayesian updating methods.

Acknowledgements

The authors wish to thank the Research Foundation - Flanders (FWO) for the financial support on the research project (Grant number 3G010220) “Vibration-based post-fire assessment of concrete structures using Bayesian updating techniques”.

References

- [1] J. Beitel and N. Iwankiw, “Historical Survey of Multi-Story Building Collapses Due to Fire,” *Fire Protection Engineering*, vol. 27, 2005.
- [2] CIB W14 Report, “Repairability of Fire Damaged Structures,” *Fire Safety Journal*, vol. 16, pp. 251–336, 1990.
- [3] B. Jovanović, R. Caspeele, G. Lombaert, E. Reynders, and R. Van Coile, “State-of-the-art review on the post-fire assessment of concrete,” *Structural Concrete*, 2023.
- [4] T. Molkens, R. Van Coile, and T. Gernay, “Assessment of damage and residual load bearing capacity of a concrete slab after fire: Applied reliability-based methodology,” *Engineering Structures*, vol. 150, pp. 969–985, 2017, doi: 10.1016/j.engstruct.2017.07.078.
- [5] D. Anastopoulos, M. De Smedt, L. Vandewalle, G. De Roeck, and E. P. B. Reynders, “Damage identification using modal strains identified from operational fiber-optic Bragg grating data,” *Structural Health Monitoring*, vol. 17, no. 6, pp. 1441–1459, 2018, doi: 10.1177/1475921717744480.
- [6] E. P. B. Reynders *et al.*, “Experimental analysis of the influence of moderate fire damage on the dynamic and incremental static behavior of reinforced concrete beams,” *Engineering Structures*, vol. 323, p. 119213, Jan. 2025, doi: 10.1016/j.engstruct.2024.119213.
- [7] B. Jovanović, R. Caspeele, E. Reynders, G. Lombaert, and R. Van Coile, “Bayesian Updating Methodology for the Post-fire Evaluation of the Maximum Temperature Profile Inside Concrete Elements,” *Fire Technol*, Mar. 2024, doi: 10.1007/s10694-024-01564-2.
- [8] CEN, “EN 1991-1-2:2002: Eurocode 1: Actions on structures - Part 1-2: General actions - Actions on structures exposed to fire.” European Standard, 2002.
- [9] CEN, “EN 1992-1-2:2004: Eurocode 2: Design of concrete structures - Part 1-2: General rules. Structural fire design.” European Standard, 2004.
- [10] T. Gernay, “A multiaxial constitutive model for concrete in the fire situation including transient creep and cooling down phases,” Doctoral thesis, Université de Liège, Belgium, 2012.
- [11] J.-M. Franssen, “Etude du comportement au feu des structures mixtes acier-béton,” Doctoral thesis, ULiège - Université de Liège, 1987.
- [12] CEN, “EN 1994-1-2:2005 Eurocode 4: Design of composite steel and concrete structures - Part 1-2 General rules - Structural fire design,” *European Standard*. European Standard, 2005.
- [13] T. Gernay and J. M. Franssen, “A formulation of the Eurocode 2 concrete model at elevated temperature that includes an explicit term for transient creep,” *Fire Safety Journal*, vol. 51, pp. 1–9, 2012, doi: 10.1016/j.firesaf.2012.02.001.
- [14] I. C. Neves, J. P. C. Rodrigues, and A. de P. Loureiro, “Mechanical Properties of Reinforcing and Prestressing Steels after Heating,” *Journal of Materials in Civil Engineering*, vol. 8, no. 4, 1996, doi: 10.1061/(asce)0899-1561(1996)8:4(189).
- [15] V. K. R. Kodur and A. Agrawal, “An approach for evaluating residual capacity of reinforced concrete beams exposed to fire,” *Engineering Structures*, vol. 110, pp. 293–306, 2016, doi: 10.1016/j.engstruct.2015.11.047.
- [16] B. Jovanović *et al.*, “Experimental investigation on the effect of natural fire exposure on the post-fire behavior of reinforced concrete beams using electric radiant panel,” *Structural Concrete*, doi: 10.1002/suco.202400550.
- [17] A. Gelman, J. B. Carlin, H. S. Stern, and D. B. Rubin, *Bayesian data analysis*. Chapman and Hall/CRC, 1995.

- [18] E. Simoen, “Uncertainty Quantification in Finite Element Model Updating,” Doctoral thesis, KU Leuven, Leuven, Belgium, 2013.
- [19] JCSS, *JCSS Probabilistic Model Code. Part 2.20 Fire*. Joint Committee on Structural Safety, 2001.
- [20] M. Colombo and R. Felicetti, “New NDT techniques for the assessment of fire-damaged concrete structures,” *Fire Safety Journal*, vol. 42, no. 6–7, pp. 461–472, 2007, doi: 10.1016/j.firesaf.2006.09.002.
- [21] P. Cioni, P. Croce, and W. Salvatore, “Assessing fire damage to r.c. elements,” *Fire Safety Journal*, vol. 36, no. 2, pp. 181–199, 2001, doi: 10.1016/S0379-7112(00)00050-3.
- [22] R. K. Chaudhary, R. Van Coile, and T. Gernay, “Potential of surrogate modelling for probabilistic fire analysis of structures,” *Fire Technology*, vol. 57, no. 6, pp. 3151–3177, 2021.
- [23] D. Anastasopoulos, P. Moretti, T. Geernaert, B. De Pauw, U. Nawrot, G. De Roeck, F. Berghmans, and E. Reynders. Identification of modal strains using sub-microstrain FBG data and a novel wavelength-shift detection algorithm. *Mechanical Systems and Signal Processing*, 86A:58-74, 2017.